Int. J. Heat Mass Transfer. Vol. 27, No. 3, pp. 419–431, 1984
Printed in Great Britain

0017–9310/84 $3.00 + 0.00

SURFACE THERMAL CAPACITY EFFECTS IN TRANSIENT NATURAL CONVECTION FLOWS AT HIGH PRANDTL NUMBER

V. P. CAREY
Department of Mechanical Engineering, University of California, Berkeley, CA 94720, U.S.A.

(*Received* 14 *February* 1983 *and in revised form* 28 *June* 1983)

Abstract—A perturbation analysis is presented for the transient natural convection flow resulting from the sudden generation of a uniform heat flux inside a vertical plate surrounded by a high Prandtl number fluid. A matched asymptotic expansion technique is used to construct time-dependent expansion solutions for flows near surfaces with zero and finite thermal capacity. Throughout the transient, the flow is found to have the same dual-layer structure which is characteristic of the steady flow at high Prandtl number (σ). The true transient regime, where surface thermal capacity effects are comparable to convection and diffusion effects, is shown to correspond to values of the parameter $\lambda = Q^*\sigma^{-4/5}$ between about 1 and 10. For large σ, the time to steady state is found to increase proportional to $\sigma^{3/5}$. Uniformly valid expansions for the velocity and temperature profiles near the surface are found to be in good agreement with calculated solutions of the full governing equations for σ as low as 16. For surfaces of small thermal capacity, a simple relation for the propagation of the leading edge effect is also obtained which is consistent with the experimental and theoretical results of previous studies at large Prandtl number.

NOMENCLATURE

A_{ij}, B_{ij} functions determined by matching
c'' thermal capacity of plate per unit surface area
g acceleration of gravity
Gr_x^* Grashof number, $g\beta q'' x^4/\nu^2 k$
k fluid thermal conductivity
Nu_x local Nusselt number, $q'' x/k(t_0 - t_\infty)$
q'' heat generation rate per unit of plate area
Q^* thermal capacity parameter, $c''(g\beta q'' \nu^2/k^5)^{1/4}$
t fluid temperature
t_0 local surface temperature
t_∞ temperature of ambient fluid far from plate
T dimensionless temperature
T_i' functions in inner expansion for T
u component of velocity parallel to surface
U dimensionless u velocity, $u/(\nu^2 g\beta q''/k)^{1/4}$
U_i' functions in inner expansion for U
U_i'' functions in outer expansion for U
v component of velocity normal to surface
V dimensionless v velocity, $v/(\nu^2 g\beta q''/k)^{1/4}$
V_i' functions in inner expansion for V
V_i'' functions in outer expansion for V
x vertical distance above the bottom of the plate
X dimensionless x coordinate, $(Gr_x^*)^{1/4}$
x_P leading edge propagation distance
X_P dimensionless leading edge propagation distance, $x_P/(\nu^2 k/g\beta q'')^{1/4}$
y horizontal distance from plate
Y dimensionless y coordinate, $y(Gr_x^*)^{1/4}/x$.

Greek symbols
β coefficient of thermal expansion
η inner stretched y coordinate, $\sigma^{1/5}Y$
θ stretched time variable, $\sigma^{-3/5}\tau$
λ thermal capacity parameter, $Q^*\sigma^{-4/5}$
ν kinematic viscosity
ξ outer stretched y coordinate, $\sigma^{-3/10}Y$
σ fluid Prandtl number
$\bar{\tau}$ time
τ dimensionless time.

INTRODUCTION

IN TECHNOLOGICAL applications where heat dissipating surfaces are cooled by natural convection, the impulsive heating of a vertical surface surrounded by fluid often gives rise to a transient natural convection flow. The importance of this type of cooling process has prompted a number of studies of the transient laminar fluid motion and heat transfer which result from the sudden generation of a uniform heat flux in a vertical plate surrounded by motionless fluid. While some early studies [1–3] neglected the effect of the surface thermal capacity, more recent investigations [4–9] indicate that appreciable surface thermal capacity can strongly affect such flows.

For the flow resulting from the sudden application of a uniform heat flux, analytical solutions have been obtained [3, 4] for the one-dimensional (1-D) portion of the transient. These results indicate that the effect of the surface thermal capacity is particularly strong during the early part of the transient. Integral methods [1, 2] and finite-difference computational schemes [7–9] have also been used to predict the transport during the entire transient, for surfaces with zero and finite thermal capacity. The results of these analyses compare favorably with the available experimental data [6, 10–12]. The propagation speed of the leading edge effect predicted by these analyses is also consistent with experimental observations [4, 5, 7, 11, 12].

Although there have been a number of previous

studies of the transient natural convection flow near a suddenly heated vertical surface, there exists little information about the systematic behavior of such flows at high Prandtl number. The finite-difference calculations [7–9], which have been made for these flows, have been at Prandtl numbers near 1, for gases, or near 7, for water. The closed-form solutions [3, 4] for the 1-D portion of the transient may be evaluated for any Prandtl number, but they are valid only for short times. Gebhart [2] presented solutions for a uniform-flux surface with finite heat capacity for values of Prandtl numbers up to 1000. However, the accuracy of these solutions is limited by the assumptions of the integral method used in the analysis.

Almost all experimental data on transient natural convection flows of this type [5, 6, 10–12] have also been from flows in fluids with Prandtl numbers near either 1 or 7. One exception is the limited observations reported by Soehngen [13] for transient natural convection near a uniform-heat-flux plate at a Prandtl number of about 10^5.

The present work is an analysis of the transient natural convection resulting from the sudden generation of a uniform heat flux inside a plate immersed in a high Prandtl number fluid. High Prandtl number flows of this type may commonly arise in engineering applications. High Prandtl number fluids are sometimes used as a heat sink in electrical transformers. The sudden application of power to the transformer produces a transient natural convection flow. The sudden heating of high Prandtl number hydrocarbon and silicone polymers during chemical processing operations will often initiate a transient natural convection flow. Similar transient flows arise in the heating of various liquid food products. Knowledge of the resulting heat transfer is often essential for these circumstances to avoid overheating the product. Transient heat input into thermal energy storage devices also may produce a transient high Prandtl number flow in the liquid phase of the storage unit.

In the analysis presented here, a matched asymptotic expansion technique, similar to that used by Carey [14], is combined with an explicit finite-difference computational scheme. Asymptotic transient profiles are obtained numerically for the limiting circumstance of $\sigma \to \infty$. First-order corrections are also computed so the results may be used to predict flow and heat transfer at large but finite values of σ. It will be shown that the results accurately predict the flow behavior at least in the range $16 < \sigma < \infty$. The major advantage of this computational technique is that once they are calculated, the results of this analysis can be used to construct complete transient solutions for any large Prandtl number using Van Dyke's [15] method of additive composition. These results also provide a more complete picture of the manner in which the heat transfer and flow behavior changes with Prandtl number as $\sigma \to \infty$. In addition, the results also indicate how the effect of the surface thermal capacity on the flow changes as σ becomes large.

ANALYSIS

The analysis applies to a flat vertical plate of finite thickness and thermal capacity, c'', immersed in an extensive body of quiescent fluid at a uniform temperature, t_∞. At time $\bar{\tau} = 0$, the plate is suddenly subjected to a constant energy input uniformly distributed over the plate. The input rate per unit surface area is q''.

Rectangular coordinates are used with the x-axis vertically upward and the origin at the bottom of the plate. The y-axis is normal to the plate with the origin at the surface. The velocity components in the x- and y-directions are u and v, respectively. The analysis incorporates the non-dimensional variables below.

$$T = \frac{t - t_\infty}{(\nu^2 q''^3/g\beta k^3)^{1/4}}, \quad \tau = \frac{\bar{\tau}}{(k/g\beta q'')^{1/2}}, \tag{1}$$

$$U = \frac{u}{(\nu^2 g\beta q''/k)^{1/4}}, \quad V = \frac{v}{(\nu^2 g\beta q''/k)^{1/4}}, \tag{2}$$

$$X = \frac{x}{(\nu^2 k/g\beta q'')^{1/4}} = (Gr_x^*)^{1/4},$$

$$Y = \frac{y}{(\nu^2 k/g\beta q'')^{1/4}} = \frac{y}{x}(Gr_x^*)^{1/4}. \tag{3}$$

The equations governing conservation of mass, momentum and energy, in terms of these non-dimensional variables, are given below. The usual Boussinesq and boundary layer approximations have been made

$$\frac{\partial U}{\partial X} + \frac{\partial V}{\partial Y} = 0, \tag{4a}$$

$$\frac{\partial U}{\partial \tau} + U\frac{\partial U}{\partial X} + V\frac{\partial U}{\partial Y} = T + \frac{\partial^2 U}{\partial Y^2}, \tag{4b}$$

$$\frac{\partial T}{\partial \tau} + U\frac{\partial T}{\partial X} + V\frac{\partial T}{\partial Y} = \frac{1}{\sigma}\frac{\partial^2 T}{\partial Y^2}. \tag{4c}$$

The initial and boundary conditions are

$$\tau = 0: \quad U = V = T = 0, \tag{5a}$$

$$X = 0: \quad U = V = T = 0, \tag{5b}$$

$$Y = 0: \quad U = V = 0, \quad Q^*\left(\frac{\partial T}{\partial \tau}\right) - \left(\frac{\partial T}{\partial Y}\right) = 1, \tag{5c}$$

$$Y \to \infty: \quad U = T = 0, \tag{5d}$$

where boundary condition (5c) results from an energy balance on the plate and Q^* is a non-dimensional parameter which depends on the plate thermal capacity and the fluid properties

$$Q^* = c''\left(\frac{\nu^2 g\beta q''}{k^5}\right)^{1/4}. \tag{6}$$

As $\sigma \to \infty$, the coefficient of the second derivative in the energy equation vanishes. Hence a singular perturbation technique is needed to obtain a solution for large σ. Following Carey [14], the flow is assumed to consist of two regions: an inner region dominated by

buoyancy and viscous forces, and an outer region where only viscous and momentum effects are important. In the inner region, the Y and time coordinates are stretched as follows:

$$\eta = \sigma^{1/5} Y, \quad \theta = \sigma^{-3/5}\tau. \tag{7}$$

Inner expansions for U, V and T are taken to be

$$U = \sigma^{-3/5}[U'_0 + \sigma^{-1/2}U'_1 + \sigma^{-1}U'_2 + \ldots], \tag{8a}$$

$$V = \sigma^{-4/5}[V'_0 + \sigma^{-1/2}V'_1 + \sigma^{-1}V'_2 + \ldots], \tag{8b}$$

$$T = \sigma^{-1/5}[T'_0 + \sigma^{-1/2}T'_1 + \sigma^{-1}T'_2 + \ldots]. \tag{8c}$$

The inner variables and expansions are chosen so that, to lowest order, as $\sigma \to \infty$, the inner momentum equation retains only the viscous and buoyancy terms.

Writing the governing equations (4a)–(4c) in terms of the inner coordinates (7) and expansions (8a)–(8c), and requiring that the equations be satisfied at each level in powers of σ, the following systems of equations are obtained

$$\frac{\partial U'_0}{\partial X} + \frac{\partial V'_0}{\partial \eta} = 0, \tag{9a}$$

$$\frac{\partial^2 U'_0}{\partial \eta^2} + T'_0 = 0, \tag{9b}$$

$$\frac{\partial T'_0}{\partial \theta} + U'_0\frac{\partial T'_0}{\partial X} + V'_0\frac{\partial T'_0}{\partial \eta} = \frac{\partial^2 T'_0}{\partial \eta^2}, \tag{9c}$$

$$\frac{\partial U'_1}{\partial X} + \frac{\partial V'_1}{\partial \eta} = 0, \tag{10a}$$

$$\frac{\partial^2 U'_1}{\partial \eta^2} + T'_1 = 0, \tag{10b}$$

$$\frac{\partial T'_1}{\partial \theta} + U'_0\frac{\partial T'_1}{\partial X} + U'_1\frac{\partial T'_0}{\partial X} + V'_0\frac{\partial T'_1}{\partial \eta} + V'_1\frac{\partial T'_0}{\partial \eta} = \frac{\partial^2 T'_1}{\partial \eta^2}. \tag{10c}$$

In the momentum equation, the lowest order convection and time derivative terms are of the same order of magnitude as the second-order correction to the viscous and buoyancy terms. Hence they do not affect the solution to this level of truncation.

In the outer region, the stretched coordinates and expansions are taken to be

$$\xi = \sigma^{-3/10} Y, \quad \theta = \sigma^{-3/5}\tau, \tag{11}$$

$$U = \sigma^{-3/5}[U''_0 + \sigma^{-1/2}U''_1 + \sigma^{-1}U''_2 + \ldots], \tag{12a}$$

$$V = \sigma^{-3/10}[V''_0 + \sigma^{-1/2}V''_1 + \sigma^{-1}V''_2 + \ldots], \tag{12b}$$

$$T \equiv 0. \tag{12c}$$

The scaling and expansions are chosen so that, to lowest order, only momentum and viscous terms are retained. The temperature field is exponentially small in the outer region and is therefore taken as zero in the expansion to $O(\sigma^{-1})$.

Substituting in the same manner as for the inner equations, the following system of equations are obtained for the outer velocity terms

$$\frac{\partial U''_0}{\partial X} + \frac{\partial V''_0}{\partial \xi} = 0, \tag{13a}$$

$$\frac{\partial U''_0}{\partial \theta} + U''_0\frac{\partial U''_0}{\partial X} + V''_0\frac{\partial U''_0}{\partial \xi} = \frac{\partial^2 U''_0}{\partial \xi^2}, \tag{13b}$$

$$\frac{\partial U''_1}{\partial X} + \frac{\partial V''_1}{\partial \xi} = 0, \tag{14a}$$

$$\frac{\partial U''_1}{\partial \theta} + U''_0\frac{\partial U''_1}{\partial X} + U''_1\frac{\partial U''_0}{\partial X} + V''_0\frac{\partial U''_1}{\partial \xi} + V''_1\frac{\partial U''_0}{\partial \xi} = \frac{\partial^2 U''_1}{\partial \xi^2}. \tag{14b}$$

Boundary conditions at the surface ($\eta = 0$) and initial conditions for the inner equations are obtained by substituting the new variables (7) and expansions (8a)–(8c) into equations (5a)–(5c). The temperature boundary condition at the surface then becomes

$$Q^*\sigma^{-4/5}\left[\frac{\partial T'_0}{\partial \theta}(X,0,\theta) + \sigma^{-1/2}\frac{\partial T'_1}{\partial \theta}(X,0,\theta) + \ldots\right] - \left[\frac{\partial T'_0}{\partial \eta}(X,0,\theta) + \sigma^{-1/2}\frac{\partial T'_1}{\partial \eta}(X,0,\theta) + \ldots\right] = 1. \tag{15}$$

Obviously, the order of magnitude of Q^* dictates the nature of this boundary condition. If $Q^* = O(\sigma^{4/5})$, then a time derivative remains in the lowest-order boundary condition. However, if Q^* is small relative to $\sigma^{4/5}$, the time derivative may be neglected. Here, two types of conditions are considered. First, if $Q^*\sigma^{-4/5}$ is less than $O(\sigma^{-1/2})$, the boundary conditions on T'_0 and T'_1 become

$$\frac{\partial T'_0}{\partial \eta}(X,0,\theta) = -1, \quad \frac{\partial T'_1}{\partial \eta}(X,0,\theta) = 0. \tag{16}$$

This applies for surfaces of negligible thermal capacity. When Q^* is of $O(\sigma^{4/5})$, the surface thermal capacity effect is comparable to convective and diffusion effects in the flow. This is the regime of 'true convection transients' described by Sammakia and Gebhart [7, 8]. For smaller values of Q^*, the response is close to a 1-D transient until steady-state temperature is achieved, which occurs relatively quickly. For very large Q^* the process begins and remains quasi-static. For $Q^* = O(\sigma^{4/5})$, λ is defined as

$$\lambda = Q^*\sigma^{-4/5}. \tag{17}$$

The boundary conditions on T'_0 and T'_1 become

$$\lambda\frac{\partial T'_0}{\partial \theta}(X,0,\theta) - \frac{\partial T'_0}{\partial \eta}(X,0,\theta) = 1, \tag{18a}$$

$$\lambda\frac{\partial T'_1}{\partial \theta}(X,0,\theta) - \frac{\partial T'_1}{\partial \eta}(X,0,\theta) = 0. \tag{18b}$$

Note that for $Q^* = \lambda = 0$, equations (18a) and (18b) reduce to equation (16). If $\lambda = 1$ and 10 are arbitrarily

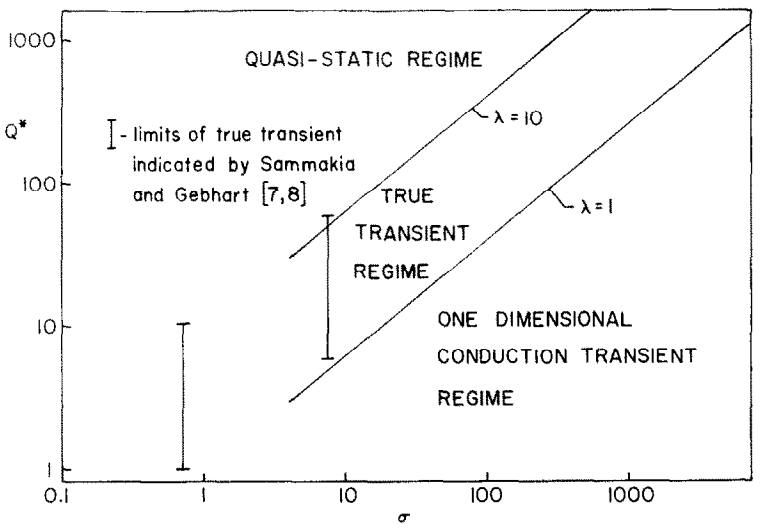

FIG. 1. The regimes of transient natural convection flow resulting from the sudden generation of a uniform heat flux in a vertical plate with finite thermal capacity.

chosen as the boundaries of conditions corresponding to true transients, it is then possible to lay out a map of the different regimes in the $\sigma - Q^*$ plane. This is done in Fig. 1. Also shown in Fig. 1 are the Q^* ranges for the true transient regime suggested by Sammakia and Gebhart [7, 8] based on their numerical calculations for $\sigma = 0.72$ and 7.6. It can be seen that the range $1 \leqslant \lambda \leqslant 10$ agrees well with the values suggested by Sammakia and Gebhart [7, 8] at these Prandtl numbers.

The boundary conditions far from the surface ($\xi \to \infty$) and the initial conditions for the outer equations are obtained by substituting the relations (11) and (12) into equations (5a), (5b) and (5d). The outer ($\eta \to \infty$) boundary conditions for the inner equations and the inner ($\xi \to 0$) boundary conditions for the outer equations are obtained by matching the inner and outer expansions. Since the inner and outer $x(X)$ and time (θ) scales are equal, the inner and outer expansions can be matched for fixed X and θ. The method used here is virtually identical to that of Carey [14]. Since the matching process is described in detail in ref. [14], only the results are presented here.

Combining the results of matching with the required conditions at $\theta = 0$, $X = 0$, $\eta = 0$ and $\xi \to \infty$, the full boundary and initial conditions for the inner and outer equations are

at $$\theta = 0: \quad U_0' = V_0' = T_0' = 0, \tag{19a}$$

$$X = 0: \quad U_0' = V_0' = T_0' = 0, \tag{19b}$$

$$\eta = 0: \quad U_0' = V_0' = 0, \quad \lambda \frac{\partial T_0'}{\partial \theta} - \frac{\partial T_0'}{\partial \eta} = 1, \tag{19c}$$

$$\eta \to \infty: \quad \frac{\partial U_0'}{\partial \eta} = T_0' = 0, \tag{19d}$$

at $$\theta = 0: \quad U_0'' = V_0'' = 0, \tag{20a}$$

$$X = 0: \quad U_0'' = V_0'' = 0, \tag{20b}$$

$$\xi = 0: \quad U_0'' = A_{00}, \quad V_0'' = 0, \tag{20c}$$

$$\xi \to \infty: \quad U_0'' = 0, \tag{20d}$$

at $$\theta = 0: \quad U_1' = V_1' = T_1' = 0, \tag{21a}$$

$$X = 0: \quad U_1' = V_1' = T_1' = 0, \tag{21b}$$

$$\eta = 0: \quad U_1' = V_1' = 0, \quad \lambda \frac{\partial T_1'}{\partial \theta} - \frac{\partial T_1'}{\partial \eta} = 0, \tag{21c}$$

$$\eta \to \infty: \quad \frac{\partial U_1'}{\partial \eta} = A_{11}, \quad T_1' = 0, \tag{21d}$$

at $$\theta = 0: \quad U_1'' = V_1'' = 0, \tag{22a}$$

$$X = 0: \quad U_1'' = V_1'' = 0, \tag{22b}$$

$$\xi = 0: \quad U_1'' = A_{10}, \quad V_1'' = B_{00}, \tag{22c}$$

$$\xi \to \infty: \quad U_1'' = 0, \tag{22d}$$

where

$$A_{00}(X, \theta) = \lim_{\eta \to \infty} U_0'(X, \eta, \theta), \tag{23a}$$

$$A_{11}(X, \theta) = \frac{\partial U_0''}{\partial \xi}(X, 0, \theta), \tag{23b}$$

$$A_{10}(X, \theta) = \lim_{\eta \to \infty} [U_1'(X, \eta, \theta) - A_{11}(X, \theta)\eta], \tag{23c}$$

$$B_{01}(X, \theta) = \frac{\partial V_0''}{\partial \xi}(X, 0, \theta), \tag{23d}$$

$$B_{00}(X, \theta) = \lim_{\eta \to \infty} [V_0'(X, \eta, \theta) - B_{01}(X, \theta)\eta]. \tag{23e}$$

Note in equations (19c) and (21c), that when $\lambda = 0$, the boundary conditions reduce to those for a surface of negligible thermal capacity (Q^* small).

The system of equations (9), (10), (13) and (14) together with the corresponding boundary and initial

conditions from equations (19)–(23) were solved numerically using an explicit finite-difference scheme. The flow region was divided into a grid with m and n spacings in the X and Y directions. Second-order derivatives were written in central differences, forward differences were used for the first-order derivatives in η, ξ and θ, and a backward difference was used for X derivatives. From a series of calculations with different grid sizes and time steps, it was concluded that $m = 20$, $n = 32$ and $\Delta\theta = 0.008$ would yield acceptable accuracy.

The value $X_{max} = 100$ was considered to represent the total height of the plate, and $\eta_{max} = \xi_{max} = 16$ were considered to represent $\eta = \infty$ and $\xi = \infty$. This is equivalent to a value of the Grashof number, Gr_x^*, of 10^8 at the end of the plate. The numerically calculated inner and outer solutions were matched in the required manner at each time step. A discussion of the details of this process may be found in ref. [14].

RESULTS AND DISCUSSION

The V-velocity and X-derivative terms in the governing equations are zero during the initial 1-D portion of the transient. This reduces the governing equations and boundary conditions to a linear system for which closed-form solutions exist. For $Q^* = \lambda = 0$, it is easily shown that the solutions for the early portion of the transient are

$$T_0' = 2\sqrt{\theta}\,\mathrm{i\,erfc}\left(\frac{\eta}{2\sqrt{\theta}}\right), \quad T_1' = 0, \tag{24a}$$

$$U_0' = 8\theta^{3/2}\left[\mathrm{i}^3\,\mathrm{erfc}\,(0) - \mathrm{i}^3\,\mathrm{erfc}\left(\frac{\eta}{2\sqrt{\theta}}\right)\right], \quad U_1' = -\theta\eta, \tag{24b}$$

$$U_0'' = 8\theta^{3/2}\,\mathrm{i}^3\,\mathrm{erfc}\left(\frac{\xi}{2\sqrt{\theta}}\right), \quad U_1'' = 0, \tag{24c}$$

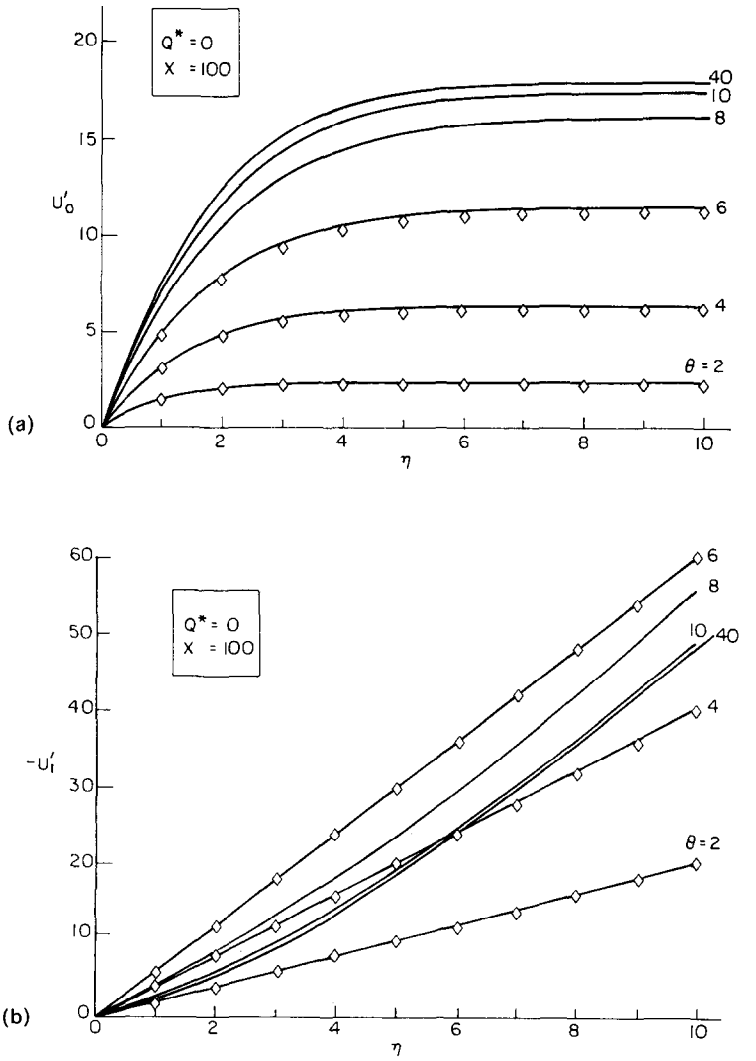

FIG. 2. (a) Calculated lowest-order and (b) first-order inner velocity profiles at various θ for $Q^* = 0$ and $X = 100$. Also shown for $\theta = 2$, 4 and 6 are the corresponding results for the closed-form solution ($\diamond$) for the early portion of the transient.

$$V_0' = V_1' = V_0'' = V_1'' = 0, \quad (24d)$$

where $i^3\,\mathrm{erfc}\,(0) = 0.0940$. The lowest-order inner and outer solutions for the U velocity can be combined using the method of additive composition [15] to obtain the following uniformly valid solution for the U velocity

$$U = 8\tau^{3/2}\sigma^{-3/2}\left[i^3\,\mathrm{erfc}\left(\frac{Y}{2\sqrt{\tau}}\right) - i^3\,\mathrm{erfc}\left(\frac{\sigma^{1/2}Y}{2\sqrt{\tau}}\right)\right] + \ldots \quad (25)$$

The uniformly-valid solution for U (25) agrees with the corresponding solution obtained by Goldstein and Briggs [4] as $\sigma \to \infty$.

The numerically calculated U_0', U_1', T_0', T_1', U_0'' and U_1'' profiles, at various θ values, are shown in Figs. 2–4 for $Q^* = \lambda = 0$ and $X = 100$. During the 1-D transient, the numerically calculated values of T_1' and U_1'' remain zero, as predicted by the closed-form solution. At $X = 100$, the leading edge effect is not felt until about $\theta = 6.5$, whereupon the solution begins to deviate from the 1-D transient behavior and T_1' and U_1'' become non-zero.

The values of T_0', U_0', U_0'' and U_1' calculated from the closed-form solutions (24a)–(24d) are also shown in Figs. 2–4, for $\theta = 2$, 4 and 6. It can be seen that the numerical calculations are in excellent agreement with the closed-form solutions for the early portion of the transient.

In Figs. 2–4, it can be seen that the U_0', T_0' and V_0'' profiles increase monotonically to their steady-state shape, except for a slight overshoot in the outer edge of the T_0' profile. However, the T_1', U_1' and U_1'' profiles overshoot their steady-state values at some locations during the transient. These results imply that the local overshoot of the temperature and u velocity during the transient diminishes with increasing Prandtl number, and, in the limit as $\sigma \to \infty$, it almost disappears.

Using the method of additive composition, the inner and outer expansions for U may be combined to form a composite expansion which is valid everywhere. Applying this technique to expansions (8a) and (12a) yields

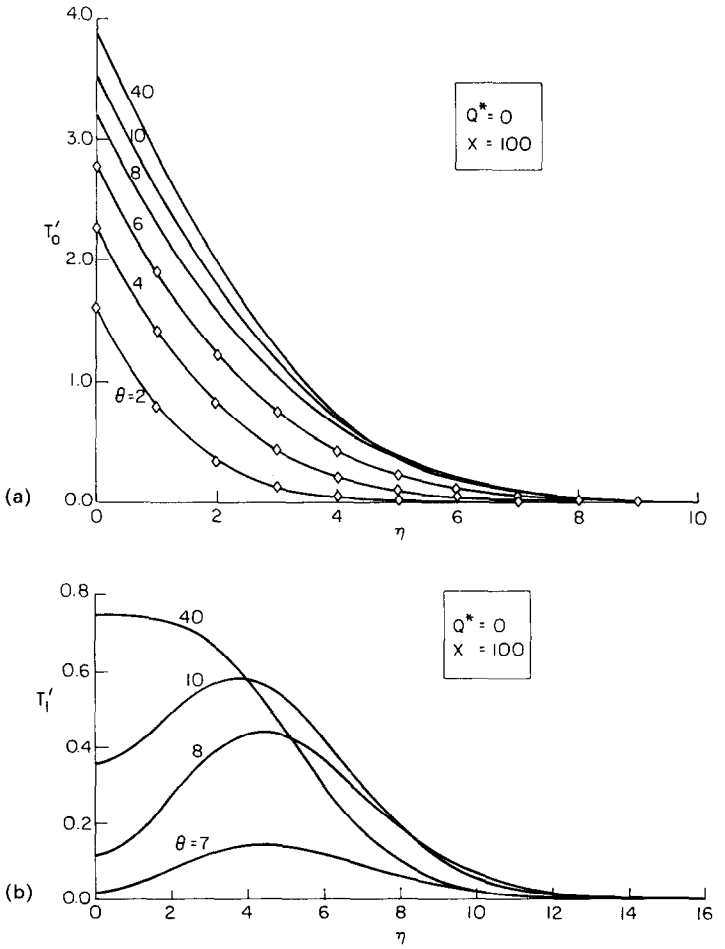

FIG. 3. (a) Calculated lowest-order and (b) first-order inner temperature profiles at various θ for $Q^* = 0$ and $X = 100$. Also shown in (a) for $\theta = 2, 4$ and 6 are the corresponding results for the closed-form solution ($\diamond$) for the early portion of the transient.

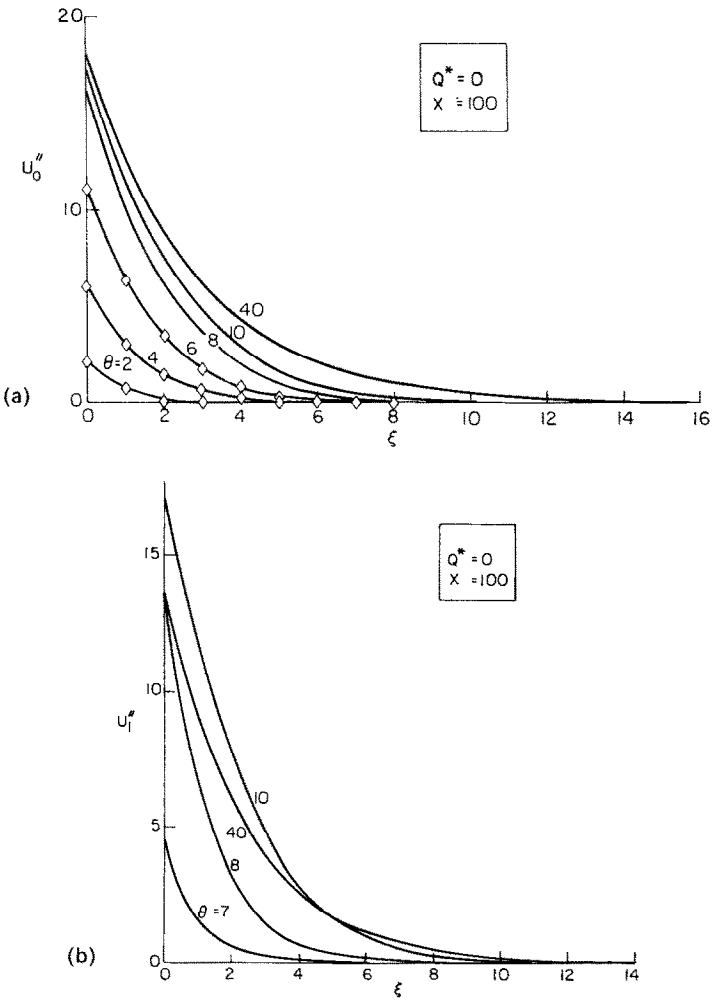

FIG. 4. (a) Calculated lowest-order and (b) first-order outer velocity profiles at various θ for $Q^* = 0$ and $X = 100$. Also shown in (a) for $\theta = 2, 4$ and 6 are the corresponding results for the closed-form solution ($\diamond$) for the early portion of the transient.

$$U \sim \sigma^{-3/5}[U_0'(X,\eta,\theta)+\sigma^{-1/2}U_1'(X,\eta,\theta)+\ldots] + \sigma^{-3/5}[U_0''(X,\xi,\theta)+\sigma^{-1/2}U_1''(X,\xi,\theta)+\ldots] - \sigma^{-3/5}[A_{00}(X,\theta)+\sigma^{-1/2}\{A_{10}(X,\theta) + A_{11}(X,\theta)\eta\}+\ldots], \quad (26a)$$

which can be rearranged to obtain the series

$$U \sim \sigma^{-3/5}[U_0'(X,\eta,\theta)+U_0''(X,\xi,\theta)-A_{00}(X,\theta) + \sigma^{-1/2}\{U_1'(X,\eta,\theta)+U_1''(X,\xi,\theta) - A_{10}(X,\theta)-A_{11}(X,\theta)\eta\}+\ldots], \quad (26b)$$

where $\eta = \sigma^{1/5}Y$, $\xi = \sigma^{-3/10}Y$ and $\theta = \sigma^{-3/5}\tau$.

Using the composite expansion (26) for the U velocity and the expansion (8c) for the temperature field, the results of the perturbation analysis were compared with the calculated solution of the original equations and boundary conditions, equations (4) and (5), for $\sigma = 16$ and $Q^* = 0$. The full solution for $\sigma = 16$ was computed using the finite-difference scheme described in the previous section, with $X_{max} = 100$, $Y_{max} = 40$, $n = 80$, $m = 20$, and a time step $\Delta\tau = 0.02$. The full solutions for U and T are shown in Fig. 5. The corresponding results of the perturbation analysis, shown as data points in Fig. 5, agree well with the full solution profiles.

The lowest-order and first-order terms in the expansions for U and T were also calculated for $\lambda = 1.0$. The resulting U_0', U_1', T_0', T_1', U_0'' and U_1'' profiles for various values of θ are shown in Figs. 6–8. Qualitatively, these profiles are similar to those obtained for $\lambda = 0$. However, the profiles approach their steady-state shapes more slowly for $\lambda = 1.0$ than for $\lambda = 0$, due to the storage of thermal energy in the surface.

For $\sigma = 16$, $\lambda = 1.0$ corresponds to $Q^* = 9.190$. The full solutions of the original governing equations, for $\sigma = 16$ and $Q^* = 9.190$, were calculated in the same manner as those for $\sigma = 16$ and $Q^* = 0$. A comparison of the resulting U and T profiles with corresponding

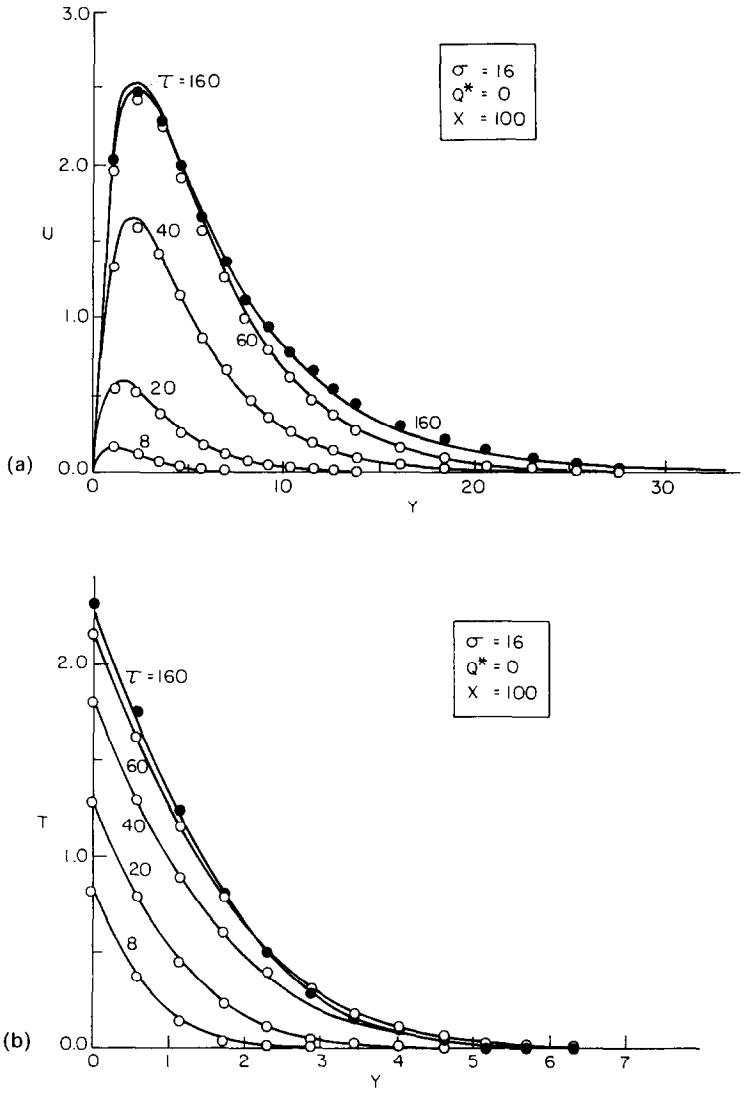

FIG. 5. (a) U and (b) T profiles calculated at various θ for $\sigma = 16$ using the full equations (—) for $Q^* = 0$ and $X = 100$. Also shown are the corresponding values calculated using the results of the perturbation analysis (○). The solid circles correspond to steady state ($\tau = 160$).

results of the perturbation analysis is shown in Fig. 9. The results of the perturbation scheme again agree well with the full solution profiles.

Using the definition of T in equation (1) together with equation (8c), one can easily show that the local Nusselt number is given by

$$Nu_x = \frac{\sigma^{1/5}(Gr_x^*)^{1/4}}{T_0'(X,0,\theta)}\left[1-\sigma^{-1/2}\frac{T_1'(X,0,\theta)}{T_0'(X,0,\theta)}+\ldots\right], \tag{27a}$$

$$\theta = \sigma^{-3/5}\tau. \tag{27b}$$

The local Nusselt number for given values of X, τ and Prandtl number can therefore be determined from equations (27a) and (27b) and the numerically determined values of T_0' and T_1' at $\eta = 0$. A major advantage of this type of analysis is that once $T_0'(X,0,\theta)$ and $T_1'(X,0,\theta)$ have been computed for various X and θ, $Nu_x(X,\theta)$ can be determined for any large Prandtl number and Gr_x^*.

Goldstein and Eckert [10] presented measurements of the transient variation of the local surface temperature resulting when a thin foil immersed in water is suddenly loaded with a uniform heat flux. Their data for one downstream (x) location are shown in Fig. 10. These data correspond to $\sigma = 6.4$, $Q^* = 0.14$ and $X = 85$. Also shown in Fig. 10 is the surface temperature variation predicted by the perturbation analysis for $\sigma = 6.4$, $Q^* = 0$, $X = 85$. It can be seen that the predicted profile agrees fairly well with the data, although it is about 7% low at steady state. However, considering the low value of Prandtl number, some deviation is

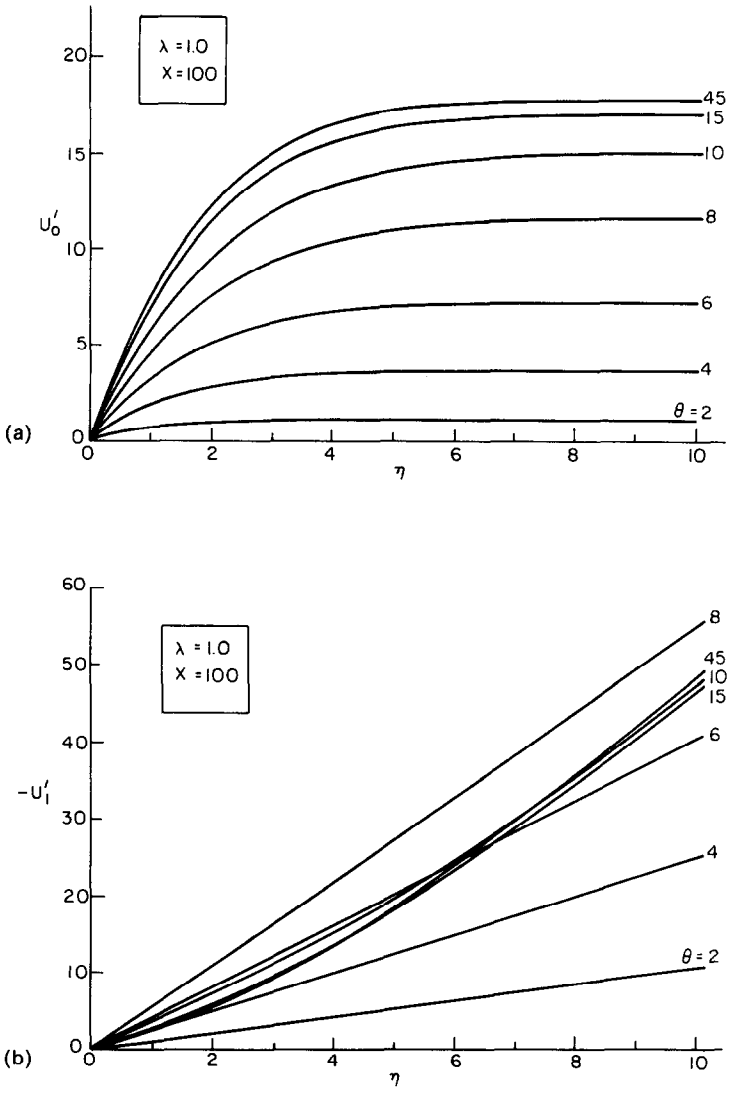

FIG. 6. (a) Calculated lowest-order and (b) first-order inner velocity profiles at various θ for $\lambda = 1.0$ and $X = 100$.

expected. The steady-state value predicted by the asymptotic analysis of Hieber and Gebhart [16] for large σ is also indicated. This result agrees with the value predicted by the present analysis within about 3%.

As indicated in Fig. 1, unless the surface thermal capacity is very large, its effect on the flow is small at large σ. Hence, in many high σ flows, λ may be taken as zero with little loss in accuracy. For $\lambda = 0$ and large σ, a simple approximation for the propagation of the leading edge effect may be determined as follows. The leading edge disturbance is assumed to propagate with the maximum u, velocity in the flow during the 1-D portion of the transient. For large σ, the maximum u velocity is taken to be that predicted by the lowest-order inner solution for U. Using equation (24b) for U_0', the following relation is obtained for u_{max}

$$u_{max} = 8i^3 \operatorname{erfc}(0)\sigma^{-3/2}(g\beta q''/k)\nu^{1/2}\bar{\tau}^{3/2}. \quad (28)$$

The maximum propagation distance of the leading edge effect is determined by

$$x_P = \int_0^{\bar{\tau}} u_{max}(\tau^*)\, d\tau^*. \quad (29)$$

Substituting equation (28) into equation (29), integrating and casting the result in dimensionless form yields

$$X_P = 0.3009\sigma^{-3/2}\tau^{5/2} = 0.3009\theta^{5/2}. \quad (30)$$

This approximate relation is plotted in Fig. 11 along with the relations for the propagation of the leading edge effect determined by Goldstein and Briggs [4] for

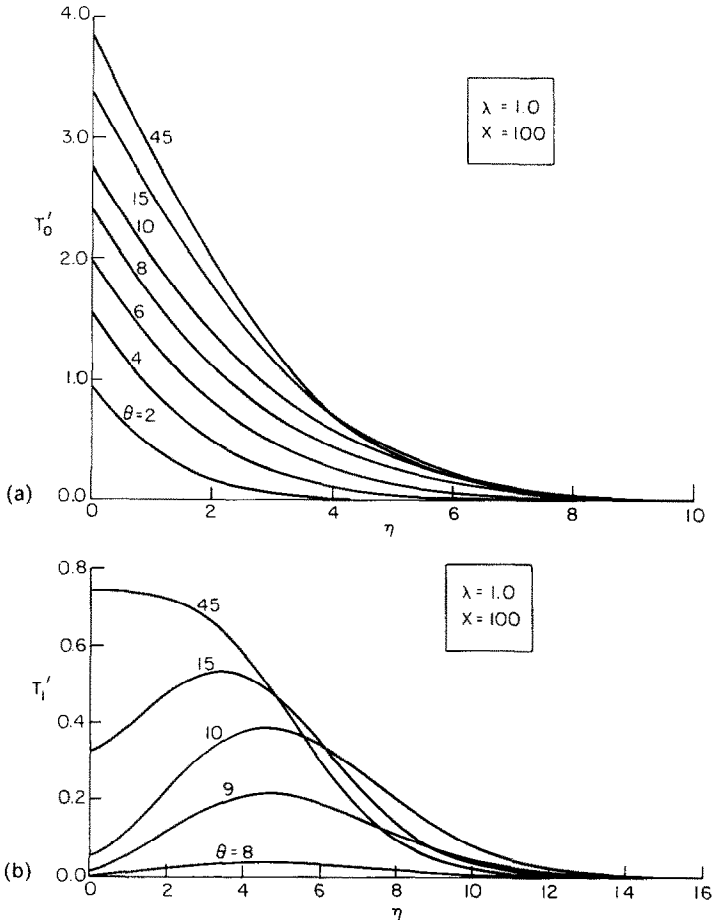

FIG. 7. (a) Calculated lowest-order and (b) first-order inner temperature profiles at various θ for $\lambda = 1.0$ and $X = 100$.

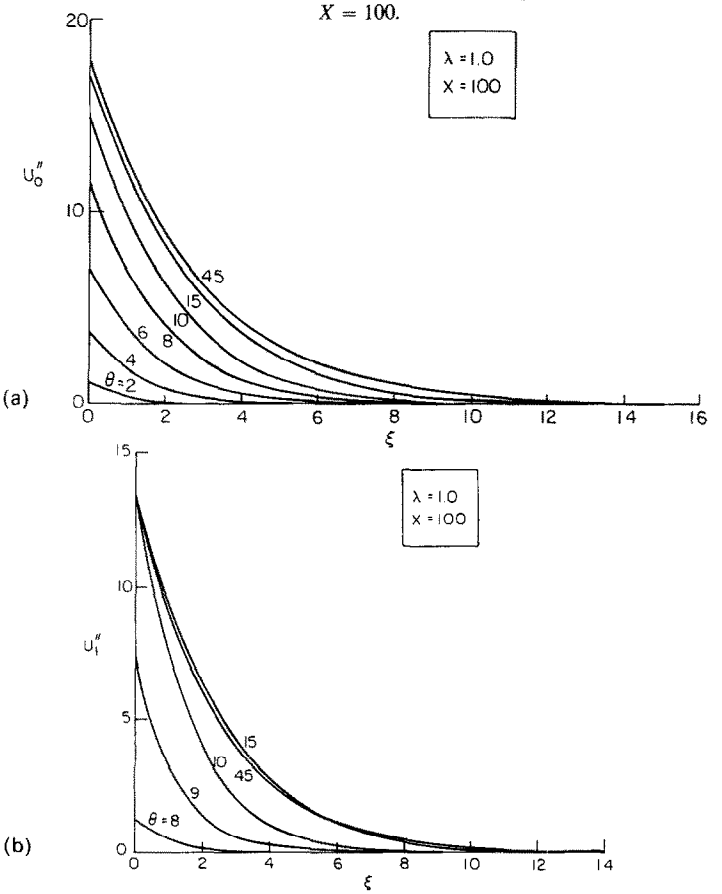

FIG. 8. (a) Calculated lowest-order and (b) first-order outer velocity profiles at various θ for $\lambda = 1.0$ and $X = 100$.

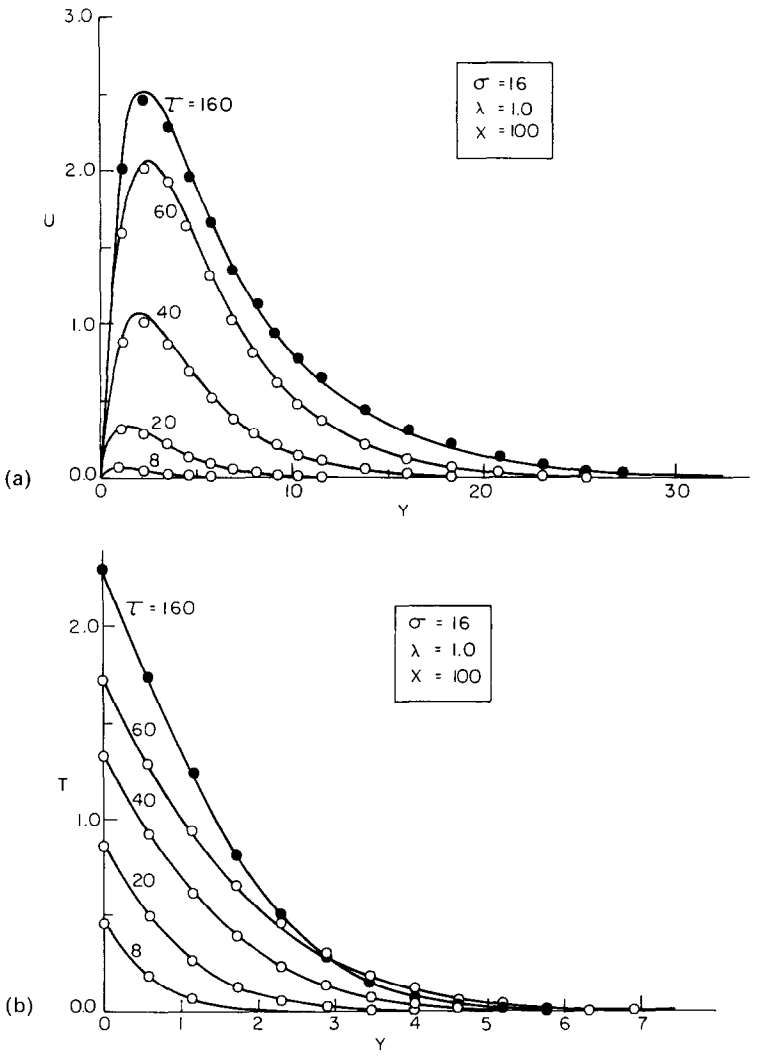

FIG. 9. (a) U and (b) T profiles calculated at various θ for $\lambda = 16$ using the full equations (—) for $\lambda = 1$ ($Q^* = 9.19$) and $X = 100$. Also shown are the corresponding values calculated using the results of the perturbation analysis (○). The solid circles correspond to steady state ($\tau = 160$).

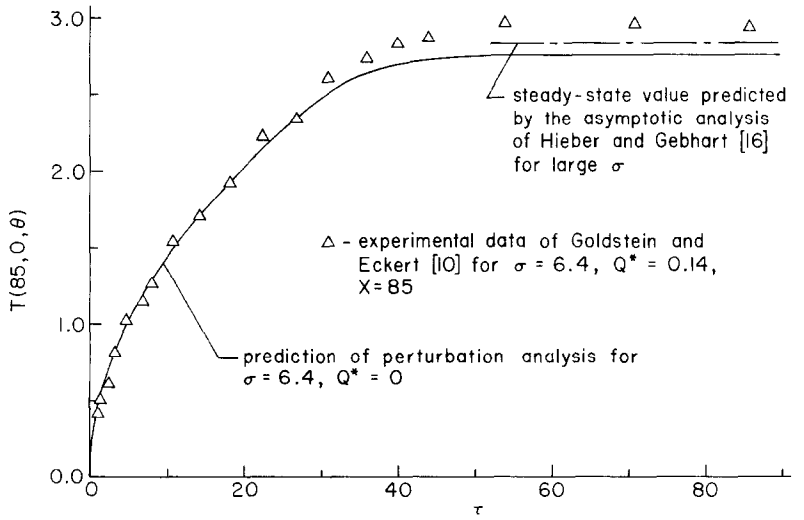

FIG. 10. A comparison of the measured surface temperature data of Goldstein and Eckert [10] for a thin heated foil in water with the temperature rise predicted by the perturbation analysis for $Q^* = 0$ at the same conditions.

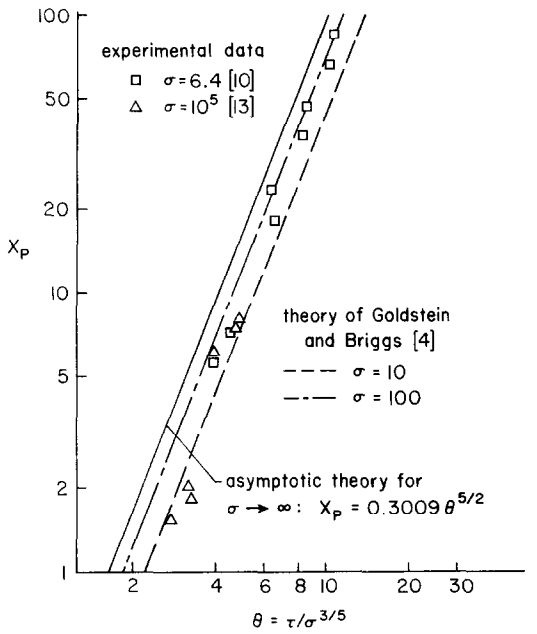

FIG. 11. The propagation of the leading edge effect predicted by the asymptotic theory for $\sigma \to \infty$ (—). Also shown are the predictions of Goldstein and Briggs [4] for $\sigma = 10$ and 100, and data from Goldstein and Eckert [10] for $\sigma = 6.4$ and Soehngen [13] for $\sigma = 10^5$.

$\sigma = 10$ and 100. Also shown are measured leading edge data from the studies of Goldstein and Eckert [10] and Soehngen [13]. The asymptotic relation (30) is consistent with the trend in the predictions of Goldstein and Briggs [4] as $\sigma \to \infty$. The experimental data confirm that scaling of τ with $\sigma^{-3/5}$ is appropriate for high Prandtl number flows. However, all the data are slightly low relative to the asymptotic relation. This slight over-prediction may be due to small surface thermal capacity effects in the experiments which are not taken into account in deriving equation (30). Nevertheless, the mathematical simplicity of equation (30) makes it attractive as an approximate method of predicting the propagation of the leading edge effect in these high Prandtl number flows.

CONCLUSIONS

At high Prandtl number, the transient natural convection flow resulting from the sudden generation of a uniform heat flux in a vertical surface is characterized by two layers. An inner region exists near the surface which is dominated by viscous and buoyancy forces, while further from the surface an outer region exists which is dominated by viscous and momentum effects. The study of Hieber and Gebhart [16] established this structure for the steady-state flow near a uniform-heat-flux surface. The present work indicates that this dual-layer structure exists throughout the transient as well.

The method of matched asymptotic expansions has been used to calculate time-dependent expansion solutions for the inner and outer regions of the flow. These may be combined to form uniformly-valid time-dependent solutions for any large Prandtl number. The two-term composite expansions were found to be in good agreement with numerically calculated solutions of the full governing equations for σ at least as low as 16.

As $\sigma \to \infty$, the results of the analysis indicate that Q^* must be of $O(\sigma^{4/5})$ for surface thermal capacity effects to be of the same magnitude as diffusion and convection effects in the boundary layer. This suggests that the true transient regime described by Sammakia and Gebhart [7, 8] corresponds to $1.0 \leqslant Q^*\sigma^{-4/5} \leqslant 10$ as $\sigma \to \infty$. Values of $Q^*\sigma^{-4/5} > 10$ correspond to the quasi-static regime, while $Q^*\sigma^{-4/5} < 1$ corresponds to the conduction transient regime. These boundaries of the true transient regime are consistent with the limiting Q^* values suggested by Sammakia and Gebhart [7, 8] at $\sigma = 0.72$ and 7.6.

For large σ, the time to steady state is proportional to $\sigma^{3/5}$. This agrees with the relation for the time to steady state obtained by Siegel [1] using an integral analysis, in the limit as $\sigma \to \infty$.

It has also been shown that the lowest-order inner solution, U'_0, provides an estimate of the propagation of the leading edge effect for $Q^* = 0$ and large σ which is consistent with the large σ trend of the theory of Goldstein and Briggs [4]. However, the approximate relation predicts a propagation speed which is slightly greater than that indicated by measurements in water [10] and a high Prandtl number polymer [13]. This slight overprediction may be due to small surface thermal capacity effects in the experiments which are neglected in this approximate prediction.

Acknowledgements—The author would like to acknowledge support from the Union Oil Foundation during the completion of this work. The efforts of Mrs J. Reed and Ms L. Donahue in preparation of this manuscript are also appreciated.

REFERENCES

1. R. Siegel, Transient free convection from a vertical flat plate, *Trans. Am. Soc. Mech. Engrs* **80,** 347–359 (1958).
2. B. Gebhart, Transient natural convection from vertical elements, *Trans. Am. Soc. Mech. Engrs*, Series C, *J. Heat Transfer* **83,** 61–70 (1961).
3. E. R. Menold and K. T. Yang, Asymptotic solutions for unsteady laminar free convection on a vertical plate, *Trans. Am. Soc. Mech. Engrs*, Series E, *J. Appl. Mech.* **29,** 124–126 (1962).
4. R. J. Goldstein and D. G. Briggs, Transient free convection about vertical plates and cylinders, *Trans. Am. Soc. Mech. Engrs*, Series C, *J. Heat Transfer* **86,** 490–500 (1964).
5. B. Gebhart and R. P. Dring, The leading edge effect in transient natural convection flow from a vertical plate, *Trans. Am. Soc. Mech. Engrs*, Series C, *J. Heat Transfer* **89,** 24 (1967).
6. B. Gebhart, R. P. Dring and C. E. Polymeropolus, Natural convection from vertical surfaces, the convection transient regime, *Trans. Am. Soc. Mech. Engrs*, Series C, *J. Heat Transfer* **89,** 53–59 (1967).
7. B. Sammakia and B. Gebhart, Transient and steady state numerical solutions in natural convection, *Numer. Heat Transfer* **1,** 529–452 (1978).

8. B. Sammakia and B. Gebhart, Transient natural convection adjacent to a vertical flat surface: the thermal capacity effect, *Numer. Heat Transfer* **4**, 331–344 (1981).
9. B. Sammakia, B. Gebhart and Z. H. Qureshi, Measurements and calculations of transient natural convection in water, *J. Heat Transfer* **104**, 644–648 (1982).
10. R. J. Goldstein and E. R. G. Eckert, The steady and transient free convection boundary layer on a uniformly heated vertical plate, *Int. J. Heat Mass Transfer* **1**, 208–218 (1960).
11. J. C. Mollendorf and B. Gebhart, An experimental study of vigorous transient natural convection, *Trans. Am. Soc. Mech. Engrs*, Series C, *J. Heat Transfer* **92**, 628–634 (1970).
12. R. L. Mahajan and B. Gebhart, Leading edge effects in transient natural convection flow adjacent to a vertical surface, *J. Heat Transfer* **100**, 731–733 (1978).
13. E. E. Soehngen, Experimental studies on heat transfer at very high Prandtl numbers, in *Progress in Heat and Mass Transfer*, Vol. 2, p. 125. Pergamon Press, Oxford (1969).
14. V. P. Carey, Analysis of transient natural convection flow at high Prandtl number using a matched asymptotic expansion technique, *Int. J. Heat Mass Transfer* **26**, 911–919 (1983).
15. M. Van Dyke, *Perturbation Methods in Fluid Mechanics*. Parabolic Press, Stanford, California (1975).
16. C. A. Hieber and B. Gebhart, Stability of vertical convection boundary layers: expansions at large Prandtl number, *J. Fluid Mech.* **49**, 577–591 (1971).

EFFETS DE CAPACITE THERMIQUE DE SURFACE EN CONVECTION NATURELLE VARIABLE A NOMBRE DE PRANDTL ELEVE

Résumé—On présente une analyse de perturbation pour la convection naturelle variable qui résulte de la création soudaine d'un flux de chaleur uniforme dans une plaque verticale dans un fluide à nombre de Prandtl élevé. Une technique de développement asymptotique est utilisée pour construire des solutions dépendant du temps pour l'écoulement près des surfaces à capacité thermique nulle ou finie. Durant la transitoire, l'écoulement a la même structure de couche duale qui est caractéristique de l'écoulement permanent à grand nombre de Prandtl (σ). Le vrai régime transitoire, celui où les effets de la capacité thermique de la surface sont comparables aux effets de la convection correspond aux valeurs du paramètre $\lambda = Q^* \sigma^{-4/5}$ comprises entre 1 et 10. Pour les grands σ, le temps d'établissement du régime permanent est proportionnel à $\sigma^{3/5}$. Des développements uniformément valables pour les profils de vitesse et de température près de la surface sont en bon accord avec les solutions des équations de base calculées pour σ aussi petit que 16. Pour des surfaces de faible capacité thermique, une relation simple pour la propagation de l'effet de bord d'attaque est obtenue et elle est en accord avec les résultats théoriques et expérimentaux d'études antérieures pour les grands nombres de Prandtl.

EINFLÜSSE DER OBERFLÄCHENWÄRMEKAPAZITÄT AUF INSTATIONÄRE NATÜRLICHE KONVEKTIONSSTRÖMUNGEN BEI HOHEN PRANDTL-ZAHLEN

Zusammenfassung—Eine Störungsanalyse wird für die instationäre natürliche Konvektionsströmung vorgelegt, die infolge der plötzlichen gleichmäßigen Beheizung einer senkrechten Platte, welche von einer Flüssigkeit mit hoher Prandtl-Zahl umgeben ist, entsteht. Um für Strömungen in der Nähe einer Oberfläche mit verschwindender oder endlicher Wärmekapazität zeitabhängige Lösungen zu finden, wird ein geeignetes asymptotisches Entwicklungsverfahren angewandt. Während des instationären Vorgangs hat die Strömung die gleiche Zweischichtenstruktur, die für die stationäre Strömung bei hohen Prandtl-Zahlen (σ) charakteristisch ist. Der tatsächliche Übergangsbereich in dem die Einflüsse der Oberflächenwärmekapazität vergleichbar sind mit denen von Konvektion und Diffusion, entspricht Werten des Parameters $\lambda = Q\sigma^{-4/5}$ zwischen ungefähr 1 und 10. Für große σ nimmt die Zeit bis zum Erreichen des stationären Endzustands proportional mit $\sigma^{3/5}$ zu. Allgemeingültige Ausdrücke für die Geschwindigkeits- und Temperaturprofile an der Oberfläche stehen in guter Übereinstimmung mit berechneten Lösungen der Bilanzgleichungen für σ bis maximal 16. Bei Oberflächen mit kleiner Wärmekapazität ergibt sich auch eine einfache Gleichung für das Fortschreiten des Fronteffekts, die mit experimentellen und theoretischen Ergebnissen früherer Untersuchungen bei hohen Prandtl-Zahlen übereinstimmt.

ВЛИЯНИЕ ТЕПЛОЕМКОСТИ ПОВЕРХНОСТИ НА НЕСТАЦИОНАРНОЕ ЕСТЕСТВЕННО-КОНВЕКТИВНОЕ ДВИЖЕНИЕ ПРИ БОЛЬШИХ ЧИСЛАХ ПРАНДТЛЯ

Аннотация—Методами возмущений рассмотрено нестационарное естественно-конвективное движение, возникающие при внезапном включении однородного теплового потока с внутренней стороны вертикальной пластины, погруженной в жидкость с большим числом Прандтля. Метод сращиваемых асимптотических разложений применяется для отыскания зависящих от времени решений для течений у поверхностей с нулевой и конечной теплоемкостью. Выяснено, что в переходном режиме поток имеет такую же двухслойную структуру, которая характерна для установившегося потока при больших числа Прандтля (σ). Показано, что действительно нестационарный режим, в котором эффекты теплоемкости поверхности сравнимы с эффектами конвекции и диффузии, соответствует значениям параметра $\lambda = Q^* \sigma^{-4/5}$ приблизительно между 1 и 10. Для больших σ время достижения стационарного состояния растет пропорционально $\sigma^{3/5}$. Найдено, что однородные разложения для профилей скорости и температуры около поверхности хорошо согласуются с полученными решениями полных уравнений для σ от 16 и выше. Для поверхностей с малой теплоемкостью найдено также простое соотношение для распространения переднего фронта, которое согласуется с экспериментальными и теоретическими результатами ранее проведенных исследований при больших числах Прандтля.